Heat, pH, and salt: synthesis strategies to favor formation of near-infrared emissive DNA-stabilized silver nanoclusters

Journal:	*ChemComm*
Manuscript ID	CC-COM-06-2023-002896.R1
Article Type:	Communication

COMMUNICATION

Heat, pH, and salt: synthesis strategies to favor formation of near-infrared emissive DNA-stabilized silver nanoclusters

Rweetuparna Guha,[a] Malak Rafik,[a] Anna Gonzàlez-Rosell,[a] Stacy M. Copp, [a,b,c]*

Received 00th January 20xx,
Accepted 00th January 20xx

DOI: 10.1039/x0xx00000x

We present chemical synthesis strategies for DNA-stabilized silver nanoclusters with near-infrared emission in the biological tissue transparency windows. Elevated temperatures can significantly increase chemical yield of near-infrared nanoclusters. In most cases, basic pH favors near-infrared nanoclusters while micromolar amounts of NaCl inhibit their formation.

DNA-stabilized silver nanoclusters (Ag_N-DNAs) are promising emitters for biosensing and bioimaging applications.[1, 2] These ultrasmall nanoparticles consist of only 10 to 30 silver atoms encapsulated by one to three single-stranded DNA oligomer templates.[3, 4] Ag_N-DNAs are reported to exhibit remarkable DNA sequence-encoded excitation and emission wavelengths[5, 6] as well as high Stokes shifts,[7] quantum yields,[8] and photostabilities.[9-11] The large combinatorial space of DNA sequence has enabled researchers to design a diverse set of Ag_N-DNAs with emission wavelengths ranging from 400 nm to 1,200 nm, far into the near-infrared (NIR).[12-17] The sequence-encoded, tunable properties of Ag_N-DNAs and their spectral sensitivity to analytes have led to chemical sensing, biosensing, and imaging applications of Ag_N-DNAs.[1, 2]

We used high-throughput experiments combined with machine learning to discover thousands of new Ag_N-DNAs.[12-16] These approaches enabled the successful design of DNA ligand sequences that stabilize Ag_N-DNAs with specific visible and NIR emission colors. NIR-emissive Ag_N-DNAs are of particular interest as novel biocompatible emitters because biological tissues and fluids scatter, absorb, and emit far less light in the tissue transparency windows.[18] The photophysical properties and atomic structures of NIR Ag_N-DNAs discovered in high-throughput experiments have since been reported in the literature.[7, 19-26] Recent work by Mastracco, *et al.* has dramatically expanded the space of known NIR-emissive Ag_N-DNAs, with over 100 10-base DNA sequences that stabilize Ag_N-DNAs with peak emission > 800 nm.[12] This large data set holds promise for rapid development of NIR-emissive Ag_N-DNAs for bioimaging applications in the tissue transparency windows.

This study is motivated by two challenges we identified regarding chemical synthesis of NIR-emissive Ag_N-DNAs. First, we and others have observed that NIR-emissive Ag_N-DNAs often take several days to a week after chemical reduction to form in appreciable quantities; in contrast, visibly emissive Ag_N-DNAs typically form within hours and up to one day.[8, 19, 24] Second, we observe discrepancies between the emission spectra of NIR Ag_N-DNAs prepared in microwell plates during high throughput experiments *versus* when individually synthesized in single microcentrifuge tubes. Many brightly emissive NIR-emissive Ag_N-DNAs identified in high-throughput experiments form with exceptionally low chemical yield or are even undetectable when prepared in single microcentrifuge tubes. In some cases, formation of visibly emissive Ag_N-DNAs by the same DNA template sequence appears to compete with formation of the NIR-emissive Ag_N-DNA of interest. To advance NIR-emissive Ag_N-DNAs for bioimaging applications, this study identifies the causes of discrepancies between microplate synthesis and microcentrifuge tube synthesis, thereby establishing chemical synthesis procedures to scale up NIR-emissive Ag_N-DNAs.

We first investigate how synthesis of NIR-emissive Ag_N-DNAs differs between microplate and microcentrifuge tube. Past work details how the robotic liquid handling routines for high-throughput Ag_N-DNA synthesis were designed for good agreement with “by-hand” synthesis of visibly emissive Ag_N-DNAs[12-16] (ESI, Section 1.2) We observe one key difference between these two methods: Ag_N-DNA samples synthesized in single microcentrifuge tubes are stored at 4 °C immediately following $NaBH_4$ reduction, except during periodic and brief fluorimetry to assess product formation. Microwell plates are exposed to room temperature for much longer periods following $NaBH_4$ reduction because fluorimetry of an entire 384-microwell plates takes ~4 hours, and plates are scanned one day and one week after reduction. Moreover, the microwell plate can rise above room temperature in the unrefrigerated plate reader. Thus, we hypothesized that heating above 4 °C favors formation of NIR-emissive Ag_N-DNAs.

[a] Department of Materials Science and Engineering, University of California, Irvine, CA 92697, USA
[b] Department of Physics and Astronomy, University of California, Irvine, CA 92697, USA
[c] Department of Chemical and Biomolecular Engineering, University of California, Irvine, CA 92697, USA
*Email: stacy.copp@uci.edu

Electronic Supplementary Information (ESI) available: Experimental details, full absorbance and emission spectra at various experimental conditions. See DOI: XXX

To test this hypothesis, we investigated how storage temperature after reduction affects Ag_N-DNA formation. Six different DNA template sequences were selected as listed in **Table 1**, with optimized concentrations of DNA and $AgNO_3$, and the peak emission wavelength(s), λ_p, of emitters produced by these templates. Sequences were chosen from a library of 10-base DNA oligomers designed using machine learning. Selection for this study is based on their formation of far-red to NIR products in high-throughput experiments.[12-16]

Table **1** AgN-DNAs with associated peak emission wavelengths, λ_p, and synthesis stoichiometries.

Name	DNA sequence (5′ to 3′)	λ_p / nm	[DNA] / µM	[AgNO$_3$] / µM
DNA-**1**	ACCGCCGGGA	680/820	25	125
DNA-**2**	CGAACCGGGC	644/820	25	187.5
DNA-**3**	AGGCGATCAT	580/844	25	187.5
DNA-**4**	GCCCCCCCGC	670	25	125
DNA-**5**	CACCCCGAGC	714	20	300
DNA-**6**	TAGCCCCTGT	562	25	125

Ag_N-DNAs were synthesized as detailed in ESI. First, a solution of $AgNO_3$ is mixed with an aqueous solution of DNA template in 10 mM NH_4OAc at pH 7, room temperature (21 °C); studies show that this forms Ag^+–DNA complexes.[27-29] Second, the sample is incubated at 21 °C for 15 minutes. Third, Ag^+–DNA complexes are reduced by freshly prepared $NaBH_4$ solution at 0.5 molar ratio to $AgNO_3$ at 21 °C. Finally, solutions are stored in the dark at four distinct conditions: 1) 4 °C for two days until measurement, the "standard" method used for single tube synthesis, 2) 37 °C for 4 hours followed by storage at 4 °C until measurement, 3) 21 °C until measurement, and 4) 37 °C for 4 hours followed by storage at 21 °C until measurement. 37 °C was chosen because well plates are warm to the touch after a 4-hour well plate scan and because thermal stability of Ag_N-DNAs at 37 °C is relevant for *in vivo* applications. Heating above 40 °C was avoided due to past evidence of irreversible conversion to larger silver nanoparticles above 40 °C.[8]

Figure 1 compares Ag_N-DNA emission spectra for the four storage conditions described above. When stored only at 4 °C, DNA-**1** forms a single dominant product with emission peak λ_p = 680 nm, but when stored at 21 °C and 37 °C for various times, a new Ag_N-DNA species with λ_p = 820 nm forms (**Fig. 1a**). Similarly, DNA-**2** displays a single λ_p = 644 nm peak when stored at 4 °C, but a new NIR-emissive Ag_N-DNA (λ_p = 820 nm) forms at higher storage temperatures (**Fig. 1b**). For both DNA-**1** and DNA-**2**, NIR peak intensity is greatest when temperature is highest: 37 °C for 4 hours followed by storage at 21 °C for the remaining 44 hours. For both DNA-**3** (λ_p = 844 nm) and DNA-**4** (λ_p = 670 nm), emission intensity of the far-red and NIR peaks exhibit *ca*. two- and three-fold increases, respectively, with increased storage temperature (**Fig. 1c**, **d**). For DNA-**3**, this increase accompanies a decrease in a minor λ_p = 580 nm peak, suggesting that a smaller Ag_N-DNA product preferentially forms at lower temperatures. These results support that increased post-reduction storage temperature enhances chemical yield of far-red to NIR-emissive Ag_N-DNAs and can even enable formation of new NIR Ag_N-DNA species that are not detectable when stored only at 4 °C. Increased storage temperature also significantly shortens the days-long to week-long incubation times reported for NIR Ag_N-DNA formation.[8, 19, 24]

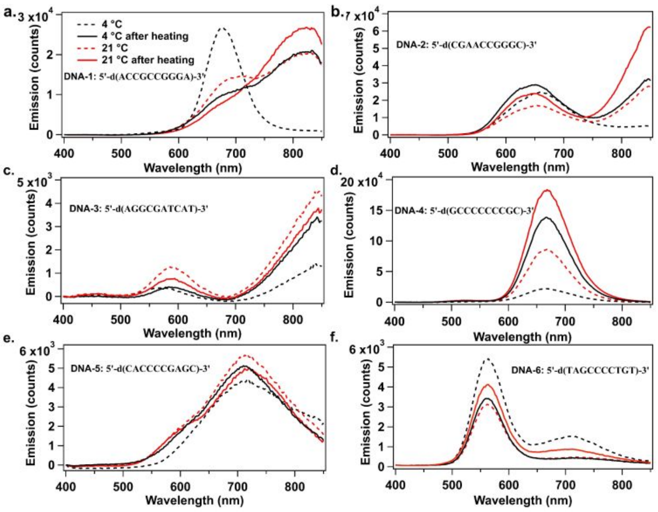

Figure **1** UV-excited emission spectra of AgN-DNAs prepared at various temperatures and recorded two days after AgN-DNA synthesis. a) DNA-**1**, b) DNA-**2**, c) DNA-**3**, d) DNA-**4**, e) DNA-**5**, and f) DNA-**6**. Samples were stored at 4 °C (dashed black), 21 °C (dashed red), 4 °C after heating at 37 °C for 4 h (solid black) and at 21 °C after heating at 37 °C for 4 h (solid red). (Fluorimetry was performed on a well plate reader with 850 nm upper spectral range; Fig. S1 shows emission spectra up to 950 nm on a different detector.)

Elevated storage temperature does not increase chemical yield of all far-red or NIR Ag_N-DNAs. Increased temperature causes a negligible increase in brightness for DNA-**5** (**Fig. 1e**). For DNA-**6**, both emissive species decreased in brightness with increased storage temperature (**Fig. 1f**). Thus, the optimum storage temperature varies among Ag_N-DNA species and should be tuned when optimizing synthesis parameters for a specific Ag_N-DNA, just as DNA and $AgNO_3$ concentrations are optimized.

Others have reported temperature effects on Ag_N-DNA synthesis. Swasey, *et al.* reported heating a red-emissive Ag_N-DNA at 40 °C to improve its chemical yield,[30] and Petty, *et al.* reported that temperature influenced absorption, excitation, and emission spectra of a NIR-emissive Ag_N-DNA by about ~20 nm.[25] We note that Vosch and coworkers have measured temperature-dependent emission spectra measurement of compositionally pure Ag_N-DNAs but that in those studies, spectroscopy was performed at various temperatures,[8, 31] while here spectra are collected at room temperature after heating.

The NIR-emissive Ag_N-DNA formed by DNA-**3** has been shown to have molecular formula $(DNA)_2[Ag_{20}]^{12+}$.[4] We used high performance liquid chromatography (HPLC) and electrospray ionization mass spectrometry (ESI-MS) (**Table S3**) to show that the λ_p = 670 nm species stabilized by DNA-**4** is $(DNA)_2[Ag_{14}]^{8+}$ (**Fig. S13**). ESI-MS supports that DNA-**6** stabilizes a λ_p = 562 nm $(DNA)_2[Ag_{12}]^{8+}$ and a NIR-emissive $(DNA)_2[Ag_{15}]^{9+}$ (**Fig. S14**). These findings agree with past reports of how Ag_N-DNA electron count correlates with fluorescence spectral properties.[32] Detailed analysis of all emitters is beyond the scope of this study.

Studies have shown that the pK_a values of deprotonable nucleobases vary over a range of 2 ΔpK_a as temperature increases from 15 to 55 °C.[33] Lee, *et al.*, reported sensing of adenosine 5′-triphosphate (ATP) by utilizing pH-dependent change in emission spectra of Ag_N-DNAs.[34] Such temperature dependence of nucleobase pK_a motivated us to next investigate how solution pH affects Ag$_N$-DNA formation. Ag$_N$-DNAs were synthesized in 10 mM NH_4OAc solutions ranging from pH 4 to 10. UV-excited emission spectra were recorded after 2 days of storage at 4 °C (ESI). **Fig. 2** shows that Ag$_N$-DNAs with visible emission peaks are brighter at acidic to neutral pH, whereas basic pH favors NIR Ag$_N$-DNAs in most cases. For example, products formed by DNA-**6** ($\lambda_p = 562$ nm) increase 6-fold in brightness at pH 6 compared to pH 7 (**Fig. 2f**). Similarly, visibly emissive products associated with DNA-**1** (λ_p = 680 nm), DNA-**2** (λ_p = 644 nm), and DNA-**4** (λ_p = 670 nm) are brightest at pH 7 (**Fig. 2a, b, d**). Preparation at basic pH can significantly increase the brightness of NIR-emissive Ag$_N$-DNAs. For DNA-**2** (λ_p = 644 nm at pH 7), the NIR emissive species (λ_p = 800 nm) increases gradually for pH > 7 (**Fig. 2b**). DNA-**4** strongly favors formation of the λ_p = 820 nm species at pH 9 (**Fig.2c**). DNA-**5** red-shifts and demonstrates increased emission intensity at basic pH (**Fig. 2e**). (Note that peak wavelengths of the NIR-emissive species for DNA-**2** differ between **Fig. 1b** and **2b**; purification and mass spectral analysis are needed to confirm if the same NIR species forms at basic pH *versus* elevated temperature.) Thus, solution pH could be exploited to dramatically increase synthesis yield of far-red and NIR-emissive Ag$_N$-DNAs. Earlier studies by Vosch and coworkers showed that the photophysical properties of both purified and non-purified Ag$_N$-DNAs stabilized by a cytosine-rich DNA oligomer are unaffected by changes in pH and ionic strength,[35] suggesting that pH does not always affect Ag$_N$-DNA formation. Further studies are required to fully understand how higher pH favors formation of NIR Ag$_N$-DNAs.

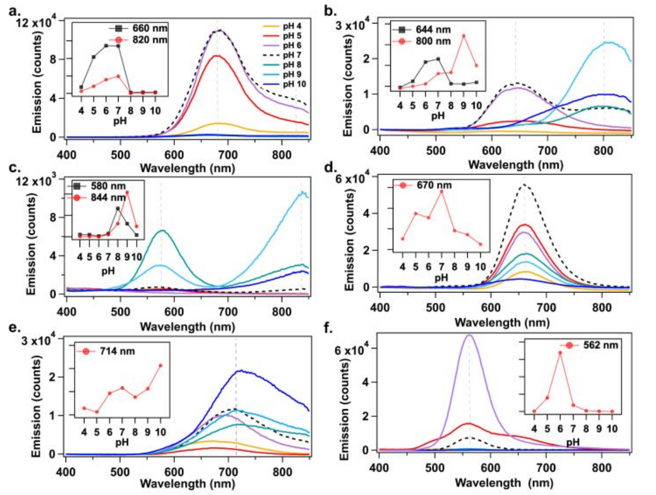

Figure 2 Changes in emission intensities of a) DNA-**1**, b) DNA-**2**, c) DNA-**3**, d) DNA-**4**, e) DNA-**5**, and f) DNA-**6** when prepared at pH 4 (yellow), 5 (red), 6 (purple), 7 (dashed black), 8 (teal), 9 (light blue), and 10 (dark blue). Insets show change in emission intensity at a specific wavelength (indicated by dashed vertical grey line in the main graph) as a function of pH. Emission spectra recorded two days after NaBH4 reduction.

Finally, we investigated the effects of small amounts of NaCl on Ag$_N$-DNA emission spectra because residual reagents from commercial nucleic acid synthesis can cause variability in batch-to-batch Ag$_N$-DNA synthesis. Chlorido ligands were recently reported on Ag$_N$-DNAs, a $(DNA)_2[Ag_{16}Cl_2]^{8+}$ and $(DNA)_2[Ag_{15}Cl]^{8+}$, even though no source of chloride was intentionally added during Ag$_N$-DNA synthesis.[24] This finding supports that residual reagents from solid-phase synthesis can significantly affect Ag$_N$-DNA product formation and may be an additional source of discrepancy between high-throughput and single-tube Ag$_N$-DNA synthesis. Here, we investigated how residual chloride influences Ag$_N$-DNA formation. The six species in **Table 1** were synthesized at their optimal storage temperature at pH 7 (**Table S2**). Two days later, NaCl was added at final concentrations of 250 µM to 1000 µM (concentrations chosen for ~10 to ~100-fold excess of chloride per nanocluster). Emission spectra were measured 1 to 6 h (1 h interval) and then 24 h and 72 h after NaCl addition. To interpret the results, we first consider DNA-**6.** **Fig. 3a** to **3e** show that DNA-**6** emission spectrum evolves over time for specific concentrations of NaCl.

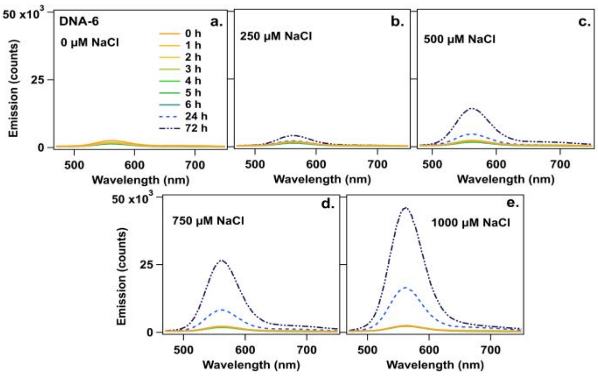

Figure **3** Emission spectra for DNA-**6** at 0 to 6, 24, and 72 h (legend) without NaCl (0 µM) and after addition of NaCl at b) 250 µM, c) 500 µM, d) 720 µM, and e) 1000 µM.

Figure 4 summarizes percent intensity change of the peak that increased most significantly with NaCl addition for each of the six DNA strands. DNA-**6** exhibits the most dramatic intensity increase with NaCl addition, up to 30-fold for 1000 µM NaCl at 72 h (**Fig. 4f**). For DNA-**1**, **2**, and **3**, which form both visible and NIR emissive species, only visible Ag$_N$-DNA species increase in emission intensity with NaCl addition (**Fig. 4a**,**b**,**c**), while associated NIR-emissive species either undergo smaller intensity increases or are unstable in the presence of NaCl (**Fig. S7**). Specific emission spectral changes in the presence of NaCl vary widely among emitters and may depend sensitively on specific nanocluster structure. For example, DNA-**4** and **5** form

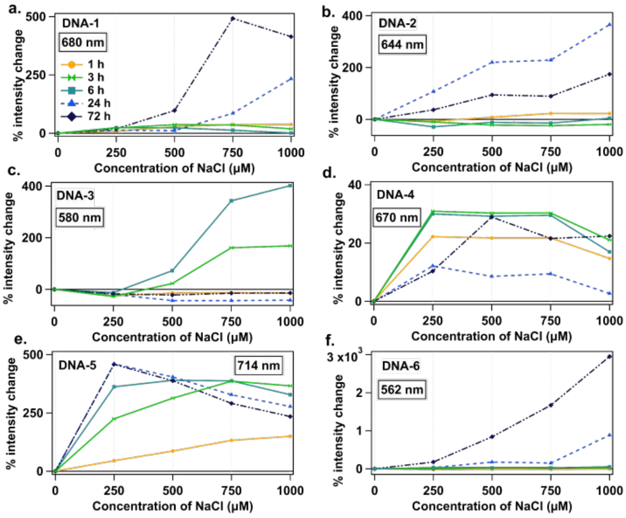

Figure **4** Percent intensity change as a function of NaCl concentration for a) DNA-**1**, b) DNA-**2**, c) DNA-**3**, d) DNA-**4**, and e) DNA-**5**, and f) DNA-**6**, specifically for the emission peak that increases the most with NaCl addition. Legend represents time points of 1 (yellow circles), 3 (green double triangles), 6 (teal squares), 24 (light blue triangles), and 72 hours (navy diamonds). Fig. S8 also shows data for 2, 4, and 5 hours.

emitters that brighten at 250 µM NaCl, whereas visible emissive species from DNA-**1**, **2** and **3** require higher NaCl concentrations (750 or 1000 µM) for significant increase. These results support that variations in residual chloride-containing reagents in commercial oligomers could contribute to discrepancies between Ag_N-DNA batches, possibly favoring formation of visible Ag_N-DNAs over NIR Ag_N- DNAs. Our ongoing research is focused on the chemical synthesis process for Ag_N-DNAs with chlorido ligands, which is beyond the scope of this study.

We hypothesize that changes in nucleobase pK_a with temperature and pH account are partly responsible for the observed changes in formation of NIR Ag_N-DNAs between microwell plate and single tube synthesis, with additional effects caused by variations in residual salts. Since the change in nucleobase pK_a with temperature and pH depends on oligomer length and the neighboring nucleobases,[33] these effects will be sequence specific and may be complex. Such sensitivity of Ag_N-DNAs to pH and halide ions could be exploited to develop novel biocompatible sensors. Future studies may determine why NIR-emissive products tend to favor basic pH and elevated temperature.

In summary, we showed how storage temperature, solution pH, and small amounts of NaCl can influence chemical yield of visible and NIR-emissive Ag_N-DNAs. Increasing the storage temperature of Ag_N-DNAs post-reduction can significantly increase emission intensity of far red and NIR Ag_N-DNAs, and in some cases is crucial to form measurable amounts of NIR-emissive Ag_N-DNAs. Basic pH promotes formation of NIR-emissive DNAs, whereas near-neutral pH favors red and far-red Ag_N-DNAs. Lastly, the presence of NaCl can significantly increase brightness of red and far-red Ag_N-DNA species. The synthesis strategies presented here are critical for the study of NIR-emissive Ag_N-DNAs, which may expedite development of promising fluorophores for NIR fluorescence bioimaging. Researchers making use of recently reported libraries of DNA template sequences for NIR Ag_N-DNAs[12, 16] should employ these synthesis methods, rather than conventional Ag_N-DNA synthesis methods which often favors smaller, visibly emissive Ag_N-DNAs.

This work was supported by NSF Biophotonics CBET-2025790. M. R. acknowledges a UC Irvine Office of Access and Inclusion Pathways to PhD Fellowship.

Conflicts of interest

There are no conflicts to declare.

Notes and references

1 Y. Chen, M. L. Phipps, J. H. Werner, S. Chakraborty and J. S. Martinez, *Acc. Chem. Res.*, 2018, **51**, 2756-2763.
2 R. Guha and S. M. Copp, in *Modern Avenues in Metal-Nucleic Acid Chemistry*, eds. J. Müller and B. Lippert, CRC Press, 2023, ch. 12, pp. 291-342.
3 A. Gonzàlez-Rosell, C. Cerretani, P. Mastracco, T. Vosch and S. M. Copp, *Nanoscale Adv.*, 2021, **3**, 1230-1260.
4 R. Guha, A. Gonzàlez-Rosell, M. Rafik , N. Arevalos, B. Katz and S. Copp, *ChemRxiv.*, 2023, DOI: https://doi.org/10.26434/chemrxiv-2023-hftx9.
5 S. M. Copp, D. Schultz, S. Swasey, J. Pavlovich, M. Debord, A. Chiu, K. Olsson and E. Gwinn, *J. Phys. Chem. Lett.*, 2014, **5**, 959-963.
6 E. G. Gwinn, P. O'Neill, A. J. Guerrero, D. Bouwmeester and D. K. Fygenson, *Adv. Mater.*, 2008, **20**, 279-283.
7 S. A. Bogh, M. R. Carro-Temboury, C. Cerretani, S. M. Swasey, S. M. Copp, E. G. Gwinn and T. Vosch, *Methods Appl. Fluoresc.*, 2018, **6**, 024004.
8 V. A. Neacşu, C. Cerretani, M. B. Liisberg, S. M. Swasey, E. G. Gwinn, S. M. Copp and T. Vosch, *Chem. Commun.*, 2020, **56**, 6384-6387.
9 J. Yu, S. Choi, C. I. Richards, Y. Antoku and R. M. Dickson, *Photochem. Photobiol.*, 2008, **84**, 1435-1439.
10 J. Yu, S. Choi and R. M. Dickson, *Angew. Chem. Int. Ed.*, 2009, **48**, 318-320.
11 S. Y. New, S. T. Lee and X. D. Su, *Nanoscale*, 2016, **8**, 17729-17746.
12 P. Mastracco, A. Gonzàlez-Rosell, J. Evans, P. Bogdanov and S. M. Copp, *ACS Nano*, 2022, **16**, 16322-16331.
13 S. M. Copp, P. Bogdanov, M. Debord, A. Singh and E. Gwinn, *Adv. Mater.*, 2016, **28**, 3043.
14 S. M. Copp, A. Gorovits, S. M. Swasey, S. Gudibandi, P. Bogdanov and E. G. Gwinn, *ACS Nano*, 2018, **12**, 8240-8247.
15 S. M. Copp, S. M. Swasey, A. Gorovits, P. Bogdanov and E. G. Gwinn, *Chem. Mater.*, 2020, **32**, 430-437.
16 S. M. Swasey, S. M. Copp, H. C. Nicholson, A. Gorovits, P. Bogdanov and E. G. Gwinn, *Nanoscale*, 2018, **10**, 19701-19705.
17 B. Sengupta, C. M. Ritchie, J. G. Buckman, K. R. Johnsen, P. M. Goodwin and J. T. Petty, *J. Phys. Chem. C*, 2008, **112**, 18776-18782.
18 G. Hong, A. L. Antaris and H. Dai, *Nat. Biomed. Eng.*, 2017, **1**, 0010.
19 A. Gonzàlez-Rosell, R. Guha, C. Cerretani, V. Rück, M. B. Liisberg, B. B. Katz, T. Vosch and S. M. Copp, *J. Phys. Chem. Lett.*, 2022, **13**, 8305-8311.
20 C. Cerretani, J. Kondo and T. Vosch, *RSC Adv.*, 2020, **10**, 23854-23860.
21 C. Cerretani, J. Kondo and T. Vosch, *CrystEngComm.*, 2020, **22**, 8136-8141.
22 M. B. Liisberg, Z. Shakeri Kardar, S. M. Copp, C. Cerretani and T. Vosch, *J. Phys. Chem. Lett.*, 2021, **12**, 1150-1154.
23 C. Cerretani, H. Kanazawa, T. Vosch and J. Kondo, *Angew. Chem. Int. Ed.*, 2019, **58**, 17153-17157.
24 A. Gonzàlez-Rosell, S. Malola, R. Guha, N. R. Arevalos, M. F. Matus, M. E. Goulet, E. Haapaniemi, B. B. Katz, T. Vosch, J. Kondo, H. Häkkinen and S. M. Copp, *J. Am. Chem. Soc.*, 2023, **145**, 10721-10729.
25 J. T. Petty, C. Fan, S. P. Story, B. Sengupta, A. S. Iyer, Z. Prudowsky and R. M. Dickson, *J. Phys. Chem. Lett.*, 2010, **1**, 2524-2529.
26 J. T. Petty, C. Fan, S. P. Story, B. Sengupta, M. Sartin, J. C. Hsiang, J. W. Perry and R. M. Dickson, *J. Phys. Chem. B*, 2011, **115**, 7996-8003.
27 J. Müller, *Coord. Chem. Rev.*, 2019, **393**, 37-47.
28 S. Naskar, R. Guha and J. Müller, *Angew. Chem. Int. Ed.*, 2020, **59**, 1397-1406.
29 J. Kondo, Y. Tada, T. Dairaku, Y. Hattori, H. Saneyoshi, A. Ono and Y. Tanaka, *Nat. Chem.*, 2017, **9**, 956-960.
30 S. M. Swasey, N. Karimova, C. M. Aikens, D. E. Schultz, A. J. Simon and E. G. Gwinn, ACS Nano, 2014, 8, 6883-6892.
31 C. Cerretani, M. R. Carro-Temboury, S. Krause, S. A. Bogh and T. Vosch, *Chem. Commun.*, 2017, **53**, 12556-12559.
32 S. M. Copp and A. Gonzàlez-Rosell, *Nanoscale*, 2021, **13**, 4602-4613.
33 J. C. González-Olvera, J. Martínez-Reyes, E. González-Jasso and R. C. Pless, *Biophys. Chem.*, 2015, **206**, 58-65.
34 J. D. Lee, J. Cang, Y.-C. Chen, W.-Y. Chen, C.-M. Ou and H.-T. Chang, *Biosens. Bioelectron.*, 2014, **58**, 266-271.
35 M. Gambucci, C. Cerretani, L. Latterini and T. Vosch, *Methods Appl. Fluoresc.*, 2019, **8**, 014005.